

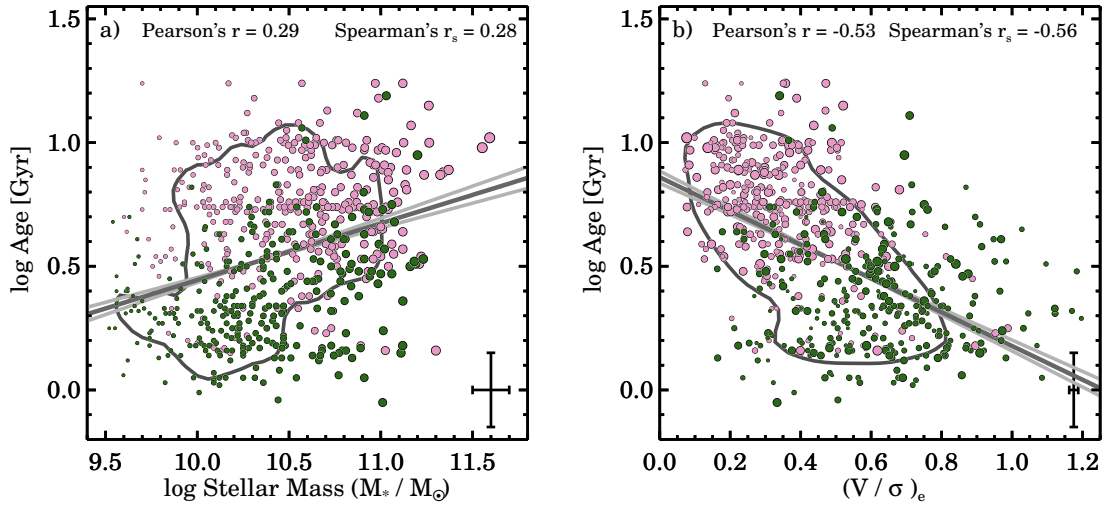


In the format provided by the authors and unedited.

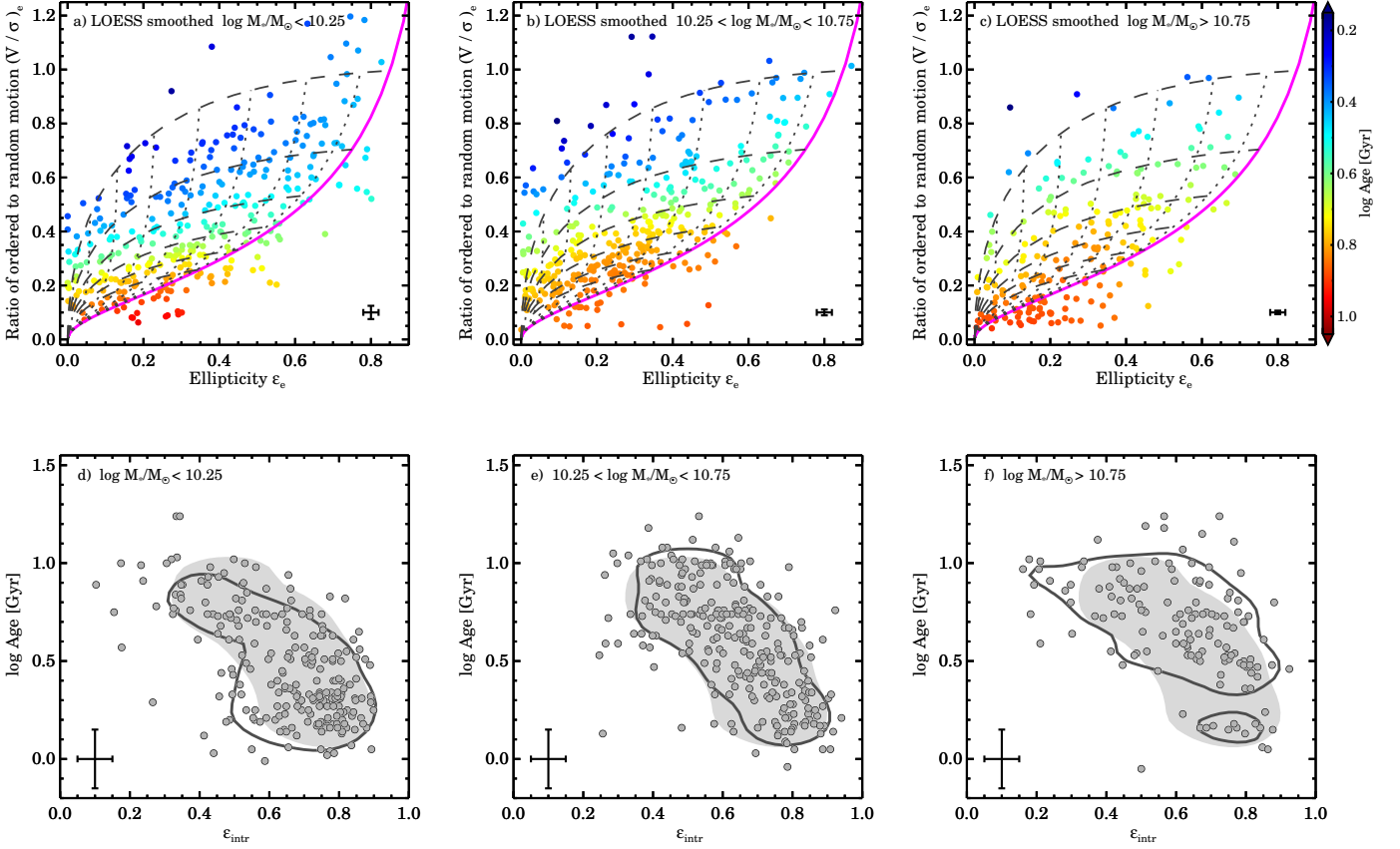
A relation between the characteristic stellar ages of galaxies and their intrinsic shapes

Jesse van de Sande ^{1*}, Nicholas Scott ^{1,2}, Joss Bland-Hawthorn¹, Sarah Brough^{2,3}, Julia J. Bryant^{1,2,4}, Matthew Colless^{2,5}, Luca Cortese⁶, Scott M. Croom^{1,2}, Francesco d'Eugenio^{2,5}, Caroline Foster^{1,7}, Michael Goodwin⁴, Iraklis S. Konstantopoulos^{4,8}, Jon S. Lawrence⁴, Richard M. McDermid^{4,9}, Anne M. Medling^{5,10}, Matt S. Owers^{4,9}, Samuel N. Richards¹¹ and Rob Sharp^{2,5}

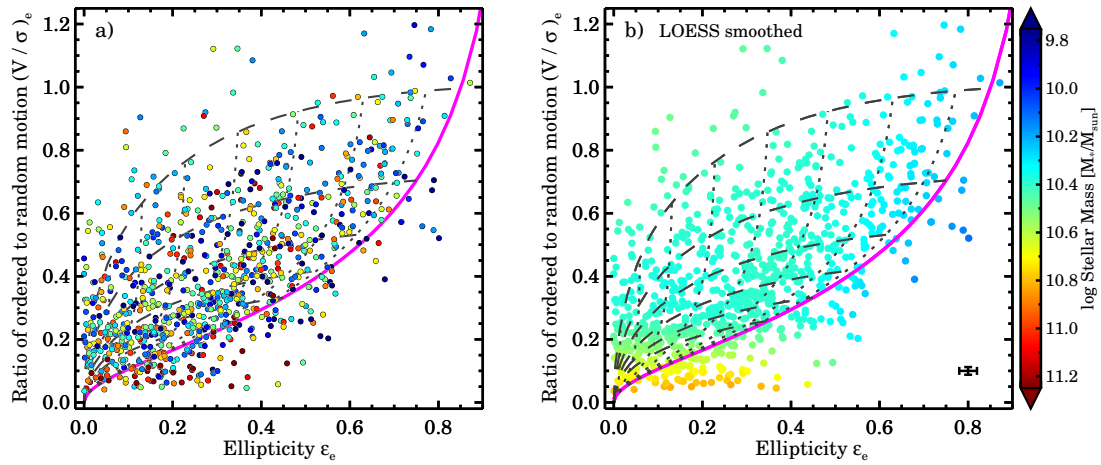
¹Sydney Institute for Astronomy, School of Physics, The University of Sydney, Sydney, New South Wales, Australia. ²ARC Centre of Excellence for All-sky Astrophysics (CAASTRO), The University of Sydney, Sydney, New South Wales, Australia. ³School of Physics, University of New South Wales, Sydney, New South Wales, Australia. ⁴Australian Astronomical Observatory, North Ryde, New South Wales, Australia. ⁵Research School of Astronomy and Astrophysics, Australian National University, Canberra, Australian Capital Territory, Australia. ⁶International Centre for Radio Astronomy Research, The University of Western Australia, Crawley, Western Australia, Australia. ⁷ARC Centre of Excellence for All-sky Astrophysics in 3 Dimensions (ASTRO 3D), The University of Sydney, Sydney, New South Wales, Australia. ⁸Atlassian, Sydney, New South Wales, Australia. ⁹Department of Physics and Astronomy, Macquarie University, Sydney, New South Wales, Australia. ¹⁰Cahill Center for Astronomy and Astrophysics California Institute of Technology, Pasadena, CA, USA. ¹¹SOFIA Operations Center, USRA, NASA Armstrong Flight Research Center, Palmdale, CA, USA. *e-mail: jesse.vandesande@sydney.edu.au



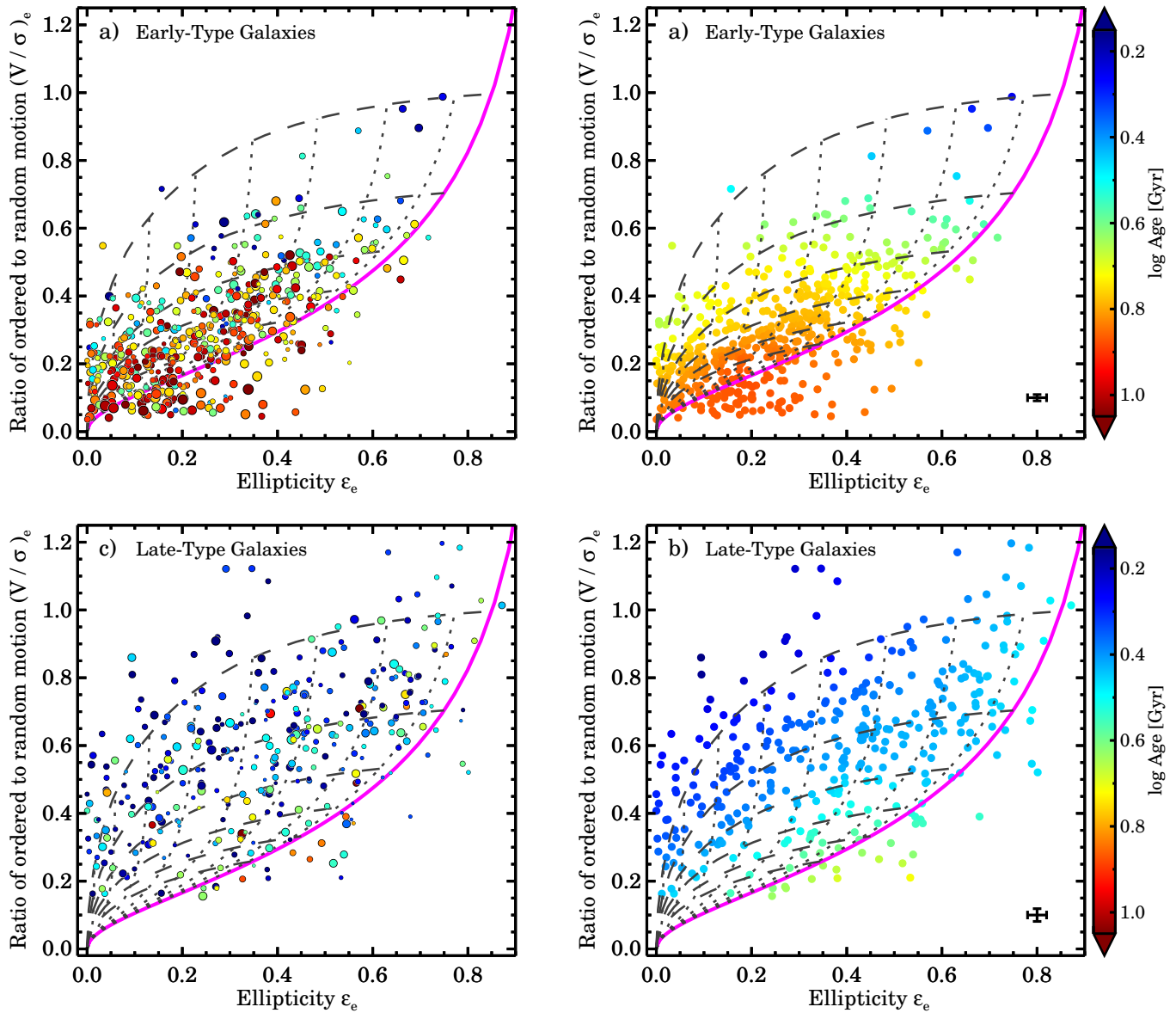
Supplementary Figure 1: **Relation between age and stellar mass in panel a) and age and $(V/\sigma)_e$ in panel b).** Sample selection is the same as in Figure 4c in the main text. Early-type galaxies are shown in pink, late-type galaxies in green. The contour encloses 68% of the total probability using kernel density estimates. We give the Pearson's and Spearman's Rank Correlation Coefficients in the top of panels a) and b). The median uncertainties are shown in the bottom-right corners. In panel a), the solid line shows the best-fitting relation of $\log \text{Age} = 0.23 \pm 0.03 \times \log_{10} M_* - 1.84 \pm 0.31$, with an RMS scatter in log Age of 0.277 dex, using the *Interactive Data Language* LINMIX_ERR function that uses a Bayesian approach to linear regression. In panel b), the solid line shows the best-fitting relation of $\log \text{Age} = -0.69 \pm 0.05 \times (V/\sigma)_e + 0.86 \pm 0.02$, with an RMS scatter in log Age of 0.245 dex. Note that the age-intrinsic ellipticity relation has less scatter (RMS = 0.238 dex) than the age-stellar mass and age- $(V/\sigma)_e$ relations.



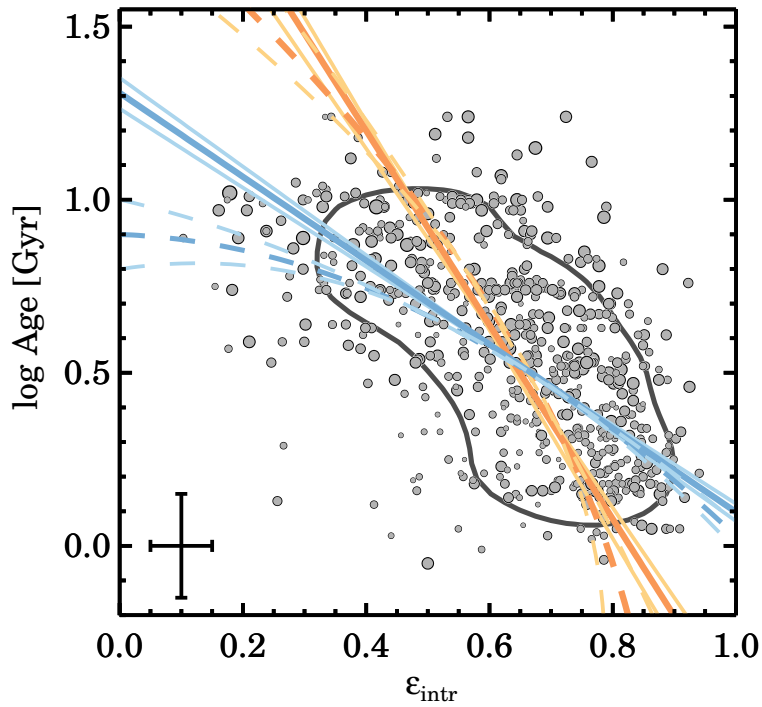
Supplementary Figure 2: **Luminosity-weighted stellar age in the $(V/\sigma, \epsilon_e)$ diagram (top-row), and log Age versus intrinsic ellipticity (bottom-row), split in different stellar mass bins.** Different columns show three different stellar mass bins, as indicated in each individual panel. The colour coding highlights the LOESS smoothed stellar population ages. The LOESS algorithm is applied separately to the three individual subsamples. The median uncertainty on $(V/\sigma)_e$ and ϵ_e are shown in the bottom-right corners, and the median uncertainty on log Age and intrinsic ellipticity are shown in the bottom-left corners. Lines shown in the top row are the same as in Figure 2 in the main text. Contours in the bottom row enclose 68% of the total probability using kernel density estimates. We find that the relation between age and intrinsic ellipticity is independent of stellar mass. Furthermore, for each mass bin we find a relation between age and intrinsic ellipticity consistent with the relation for the full sample (grey filled region). The high-mass bin has a larger fraction of old galaxies, but the distribution of points is consistent with the full sample.



Supplementary Figure 3: **Linking stellar dynamics (V/σ) and observed shape (ellipticity ϵ_e) with total stellar mass.** In panel a) the colour coding reflects low stellar mass (blue) and high stellar mass (red), whereas in panel b) we use the LOESS smoothing algorithm to look for a mean underlying trend in stellar mass. The median uncertainty on $(V/\sigma)_e$ and ϵ_e is shown in the bottom-right corner of panel b), and the median uncertainty on log stellar mass is ± 0.1 dex. Lines shown are the same as in Figure 2 in the main text. We find no trend with stellar mass for galaxies above the magenta line, i.e., objects that are consistent with being axisymmetric rotating oblate spheroids. However, galaxies with the highest stellar mass are more likely to be pressure supported spheroids than rotating.



Supplementary Figure 4: **Luminosity-weighted stellar age in the $(V/\sigma, \epsilon_e)$ diagram, split by visual morphological type, as described in Figure 3 but now including stellar population age of each individual galaxy on the left, and the LOESS smoothed stellar population ages on the right.** Galaxies with early-type morphology (Es and S0s) are shown in the top row, galaxies with late-type morphology (Sa-Sd, irregulars) are shown bottom row. The median uncertainty on $(V/\sigma)_e$ and ϵ_e is shown in the bottom-right corner, and the median uncertainty on \log age is ± 0.15 dex. Lines shown are the same as in Figure 2 in the main text. The LOESS algorithm is applied separately to the two individual subsamples.



Supplementary Figure 5: **Age versus intrinsic ellipticity.** The contour encloses 68% of the total probability using kernel density estimates. The median uncertainty on log Age and intrinsic ellipticity is shown in the bottom-left corner. The blue solid and dashed lines show the best-fitting relations as described in Figure 4c in the main text, where we minimised the scatter in log Age (vertical). If we minimise the scatter in intrinsic ellipticity (horizontal), then we obtain: $\epsilon_{\text{intr}} = -0.37 \pm 0.03 \times \log \text{Age} + 0.84 \pm 0.01$ (solid orange line), with an RMS scatter in ϵ_{intr} of 0.138, and $\epsilon_{\text{intr}} = -0.12 \pm 0.07 \times \log \text{Age}^2 - 0.19 \pm 0.08 \times \log \text{Age} + 0.79 \pm 0.02$ (dashed orange line) with an RMS scatter in ϵ_{intr} of 0.136.